Engineering Structures 195 (2019) 414–424

Contents lists available at ScienceDirect

Engineering Structures

journal homepage: www.elsevier.com/locate/engstruct

Investigation on wind-induced aero-elastic effects of tall buildings by wind tunnel test using a bi-axial forced vibration device

Weiwei Song[a,b], Shuguo Liang[a,*], Jie Song[a], Lianghao Zou[a], Gang Hu[c]

[a] School of Civil Engineering, Wuhan University, Wuhan 430072, PR China
[b] School of Civil and Transportation Engineering, NingBo University of Technology, Ningbo 315211, PR China
[c] Centre for Wind, Waves and Water, School of Civil Engineering, The University of Sydney, Sydney, NSW 2006, Australia

ARTICLE INFO

Keywords:
Tall building
Wind load
Bi-axial forced vibration
Aero-elastic effect
Wind-induced vibration

ABSTRACT

Wind-induced vibrations of tall buildings certainly change wind effects on the structures, which is the so-called aero-elastic effect. To date, the approach to identify the aero-elastic effect is still sparse. In this paper, a bi-axial forced vibration device is developed to evaluate the aero-elastic effects of tall buildings via wind tunnel tests. The device can simulate the first-order bi-axial vibration of building models. Furthermore, the surface pressure and the top displacement of the oscillating model can be synchronously measured. The aerodynamic damping ratio and aerodynamic stiffness were identified through analyzing the aero-elastic force acting on the oscillating model. The effects of aero-elastic parameters on wind-induced responses and equivalent static wind loads of a 347 m tall building were examined and analyzed. The results show that for a return period of 100 years, the aerodynamic damping is positive while the aerodynamic stiffness is negative. Aerodynamic stiffness is much smaller than the structural stiffness and therefore it has a negligible effect on natural frequency of the building. Considering the aero-elastic effects, the maximum top displacement and acceleration decrease by approximately 4% and 10% respectively, and meanwhile, the base shear and base moment induced by equivalent static wind loads decrease by approximately 1%. This investigation indicates that wind tunnel test using such kind of bi-axial forced vibration device is an effective approach to identify aero-elastic parameters of tall buildings and even other tall slender structures.

1. Introduction

The aerodynamic elastic effects induced by aero-elastic parameters, especially by aerodynamic damping ratio, should be considered when evaluating wind-induced responses of tall slender buildings with low frequency and damping ratio [1,2]. Currently, there are mainly two types of methods to investigate the aero-elastic effect by wind tunnel tests: the aero-elastic test [2–7] and the forced vibration test [8–11]. In the former method, the aerodynamic damping ratio is identified based on the random structural responses. The results from this method, however, are highly discrete. Moreover, the results identified by different technique are varied, and meanwhile, the identified results greatly depend on the selection of sample [1]. Compared with the aero-elastic wind tunnel tests, the forced vibration wind tunnel tests possess a number of advantages including large signal-to-noise ratio, simple recognition algorithm and high recognition stability [12].

In the late 1980s, Steckley [12] designed a pivot mode activator, based on which a pendulum model can perform harmonic vibrations around the bottom axis with a given frequency and amplitude. This device was the first one to be used to identify aerodynamic elastic parameters of tall buildings. The influence of the harmonic motion with different amplitudes and frequencies on aerodynamic force coefficients and spectra of tall buildings with a square section was analyzed by a multi-point pressure measurement wind tunnel test in Canada [9]. Chen et al. have identified the aero-elastic force coefficients using time-domain method [10]. Copper et al. have identified the aerodynamic damping ratio of a tall building model with a tapered cross-section and beveled corners [11]. Katagiri et al. studied motion-induced wind forces of a rectangular tall building with side ratio of 2 [13]. A forced vibration method, which creates across-wind and torsional vibration separately, was also used in this study. It was found that the motion-induced modal wind forces are nearly in proportion to the vibration amplitude except in the reduced wind speed of 5. They also proposed a spectral analysis method and a time history analysis method to estimate wind responses of tall buildings using the motion-induced forces [14]. It should be mentioned that these studies considered only unidirectional

* Corresponding author.
E-mail address: 530395292@qq.com (S. Liang).

https://doi.org/10.1016/j.engstruct.2019.06.008
Received 27 December 2018; Received in revised form 31 May 2019; Accepted 4 June 2019

or one-dimensional aero-elastic effects, mostly examined aero-elastic parameters in the crosswind direction, or in the along-wind or cross-wind direction separately. In fact, the aero-elastic effects in the two translational directions are correlated and even coupled, in particular for tall slender buildings with a non-circular cross section under oblique wind directions [15].

In the present study, a bi-axial forced vibration device is proposed to simulate the first-order bi-axial vibrations of tall buildings. The aero-elastic parameters are identified from the surface pressure and displacement responses measured by the scan valves and laser displacement meter respectively in the wind tunnel. Furthermore, wind-induced dynamic responses and equivalent static wind loads are evaluated by an improved calculation method. This method considers the aero-elastic effects induced by building motion and hence it is more accuracy.

2. Tall building description

Changsha Shimao Plaza is a tall building with a height of 347 m (80 stories) and a 48 m × 48 m square cross-section with chamfered corners. The average mass density of the building is $\rho_s = 212\,kg/m^3$. The main structure is a core barrel-steel tube column frame structure. The first mode with a frequency of 0.175 Hz is the first order translational vibration mode in the X-axial direction; the second mode with a frequency of 0.190 Hz is the first order translational vibration mode in the Y-axial direction; the third mode with a frequency of 0.339 Hz is the first order torsional vibration mode around the central vertical axis. The mode shapes of the first three modes are shown in Fig. 1. The definition of X and Y axes is shown in Fig. 2. According to Chinese code [16], the structural damping ratios for the first three modes are set to be 0.02.

3. Wind tunnel test

3.1. Wind field and building model

Wind tunnel tests were carried out in the WD-1 wind tunnel at Wuhan University, China. The length of the test section is 16 m and the cross-sectional size is 3.2 m × 2.1 m. The geometric scale of the model was λ_L = 1:400, the frequency scale was λ_f = 20:1, the wind speed scale was λ_v = 1:20. The model was made of acrylic frames, and the coat was made of aviation light wood. On the model's surface, 256 pressure transducers were arranged at 10 layers in total, as shown in Fig. 3. There were grooves on the east and west building faces from the top to the bottom, while the north and south faces were relatively flat. Because the building is symmetric regarding to the north-south and east-west axes, wind tunnel tests were carried out only in wind directions of 90° and 180°.

According to Chinese code [16], the wind field of terrain C was

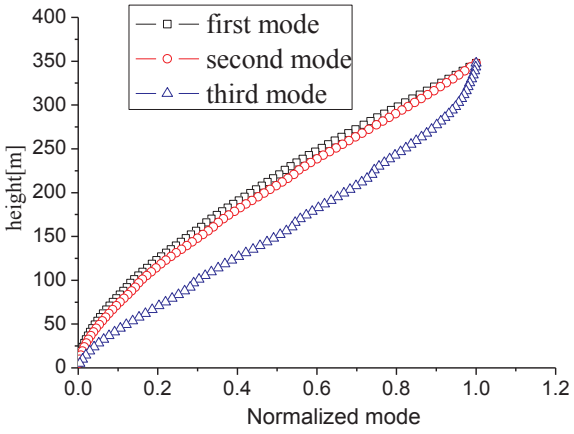

Fig. 1. Mode shapes of structure.

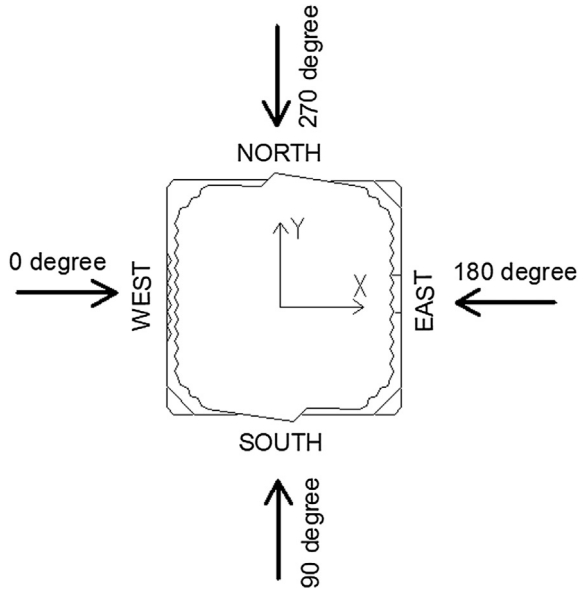

Fig. 2. Definition of coordinate system and wind directions.

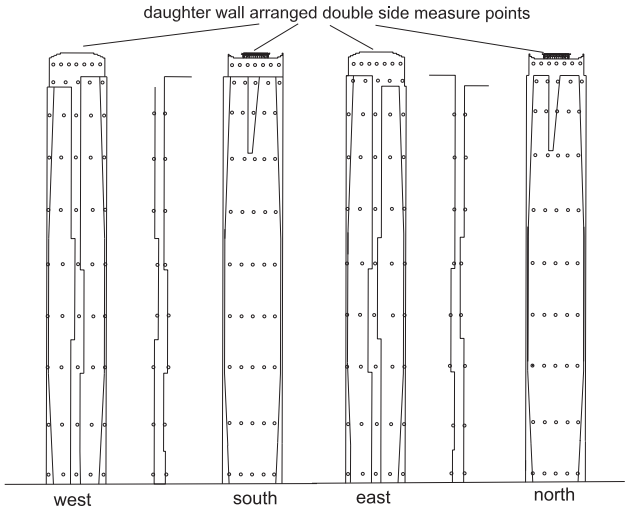

Fig. 3. The arrangement of measure transducers.

simulated in the wind tunnel. The mean wind speed profile, turbulence intensity profile and normalized wind velocity spectrum measured in the upstream of the model are shown in Fig. 4. In Fig. 4, H is the height of gradient wind; V_H is wind speed at H; V_z is wind speed at height z; α is the exponent of wind profile law; I_u is turbulent intensity; n is frequency; and $\frac{nS_V(n)}{\sigma^2}$ is dimensionless wind speed spectrum.

3.2. Bi-axial forced vibration device

The bi-axial forced vibration device used in the experiment can drive the building model to oscillate in along-wind and cross-wind directions simultaneously, following the designated frequency and amplitude. The bi-axial forced vibration mechanism in the wind tunnel tests is sketched in Figs. 5 and 6. Two wheels are driven by two DC motors separately and their rotations force sliders to move forward and backward. The translations of the connection poles fixed with the sliders are then transformed into swing of the rod attached to a traveling table at the center of the mechanism. As a result, a building model mounted on the rod vibrates harmonically with the sliders. The rod is connected to the wind tunnel floor by a spherical hinge. The vibration frequency is set by modulating the rotation speed of the wheel, while

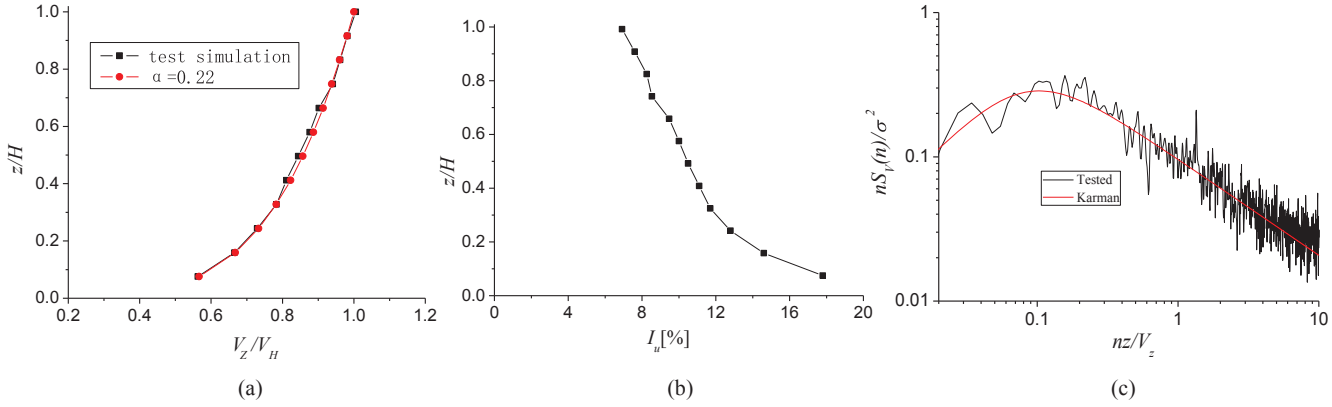

Fig. 4. Simulation of terrain C: (a) mean wind speed profile; (b) turbulence intensity profile; and (c) normalized wind velocity power spectrum.

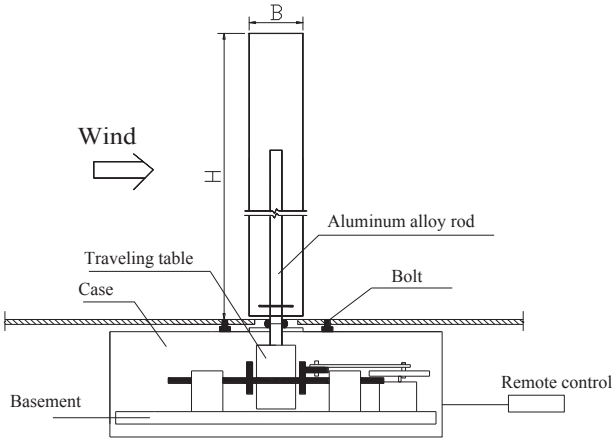

Fig. 5. Sectional view of bi-axial forced vibration apparatus.

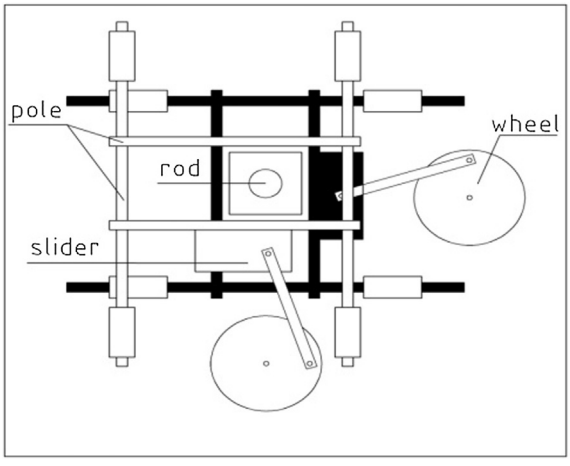

Fig. 6. Principal structure of the mechanism.

the amplitude is set by modulating the length of the crank on the wheel by a small stepping motor. Meanwhile, the phase between the vibrations of the rod in the two orthogonal directions is set up by designating the initial positions of the pole in the two directions.

The bi-axial forced vibration device is fixed underneath the wind tunnel floor as shown in Fig. 5. The working principle of the device described above was also detailed by Liang et al. [17]. The model is connected to the vibration table by the center rod. When the vibration table performs simple harmonic vibration according to the designated frequency and amplitude, the building model swings along the two main axes simultaneously. The building model mounted on the bi-axial

Fig. 7. Force vibration wind tunnel test photo.

forced vibration device in the wind tunnel is shown in Fig. 7.

The three dimensional pulsating wind velocity probe of Cobra Probe 100 (Australian TFI) was used to measure the wind velocity. The surface wind pressure of the model was measured by the DECnet Electronic Scanning Valve Pressure Measurement System (American PSI). The vibration displacement was measured by a LK-C400 laser displacement meter (Keyenee, Japan). The sampling frequencies of displacement and wind pressure are 625 Hz and 331 Hz respectively with a sampling duration of 100 s. Because the data acquisition systems of wind pressure and displacement are not compatible, the simultaneous sampling point of wind pressure and displacement is determined by “blow method”. The first step of the “blow method” is to blow air at the input end of a pipe system, and then the flow is split by a three-way shunt. The two flow pipes of the outlet end are connected with one channel of a scanning valve and a gas pressure sensor with single point respectively. The blow signals via the scanning valve and the gas pressure sensor turn into voltage signals respectively, and enter Initium Acquisition System and Ni DQmax Acquisition System respectively. The voltage signals from the gas pressure sensor are parallelly connected with the voltage signals from the laser displacement meter. Then, blow voltage signals turn into two digital pulses by both Initium Acquisition System and Ni DQmax Acquisition System respectively. According to the locations of the two pulses at the time histories of wind pressures, the synchronism of wind pressure and displacement can be determined. A computer program was developed to resample the original displacement data, and after resampling, the displacement and wind pressure data of the same sampling frequency of 331 Hz were obtained. The 3-dimensional pulsating wind speed cobra probe was placed at a height of 1000 mm, and locates at the left front of the building model with a distance of 1.3 m. The test wind speed ranged from 2 to 8 m/s, and the increment was 1 m/s. The laser displacement meter was installed at 400 mm distance

Table 1
Test cases.

	Wind direction	f_x [Hz]	f_y [Hz]	x_0 [cm]	y_0 [cm]
Case one	Direction of 180° (there is dents on the windward surface)	3.5	3.8	0.76	1.51
Case two	Direction of 90° (smooth on the windward surface)	3.5	3.8	1.51	0.76

from the building model, 500 mm height from the ground, within the effective measuring range.

The test conditions are listed in Table 1, where f_x, f_y, x_0 and y_0 are the x-axial, y-axial vibration frequencies and amplitudes at the top of the model respectively.

4. Analysis of test data

4.1. Basic assumption of aerodynamic force

For simplicity, uniform mass distribution along the structural height is assumed for the rectangular high-rise building model. In addition, the vibration mode shape of the model is assumed to be linearly distributed along the height. Taking vibration along the X-axis as an example, the equation of motion of the model is

$$m(z)\ddot{x}(z,t) + c_X(z)\dot{x}(z,t) + k_X(z)x(z,t) = F_X(x,\dot{x},z,t) \tag{1}$$

The right side of the above equation is wind force acting on the vibration model, which includes the random fluctuating wind load and the aero-elastic force. Because air density is very small compared with the building density, the influence of aerodynamic mass force can be neglected. The basic assumptions of wind loads on the model are presented as follows:

I. Load components are independent of each other. Hypothetically, the dynamic load acting on the structure consists of two parts: one is the random wind load, and the second is the aeroelastic force acting on the structure due to the change of the wind field caused by the structural movement. The correlation between them is very small, i.e., they are independent. Therefore, the wind load $F_X(x,\dot{x},z,t)$ can be expressed as a summation of a random wind load and an aerodynamic elastic force.
II. The aero-elastic forces are linear to structural movement. It is assumed that the forces generated by structural motion can be linearly expressed in terms of displacement and velocity. Because air density is very small compared with the building density, the influence of aerodynamic inertia force can be ignored. The item associated with structural displacement is called aerodynamic stiffness force item, and the item associated with structural velocity is called aerodynamic damping force term.

Based on the above two assumptions, the most classical model for aerodynamic elasticity analysis can be established, which is also based on the Scanlan classical model describing bridge flutter [18]. After employing the above two assumptions, Eq. (1) can be rewritten as follows

$$\begin{aligned} &m(z)\ddot{x}(z,t) + c_x(z)\dot{x}(z,t) + k_x(z)x(z,t) \\ &= \frac{1}{2}\rho U^2 BH\left\{C_{\mathrm{LW}}(z,t) + K_{Lx}\frac{x(t)}{x_0} + C_{Lx}\frac{\dot{x}(t)}{\omega x_0}\right\} \end{aligned} \tag{2}$$

where $C_{\mathrm{LW}}(z,t)$ represents the X-axial fluctuating wind pressure coefficients; K_{Lx} and C_{Lx} are aerodynamic stiffness force coefficient and aerodynamic damping force coefficient respectively, which are the functions of the dimensionless wind speed. The form of the function is determined exclusively by the building shape (section shape and aspect ratio), regardless of structural vibration characteristics.

4.2. Time domain integral method (TDIM) for identification of aero-elastic parameters

Assuming that the structure performs bi-axial harmonic vibrations, when the wind direction is 90° (X axis is the across-wind direction, and Y axis is the along-wind direction), the displacements in the directions of x and y axes are expressed as $x(t) = x_0\sin(\omega_x t)$, $y(t) = y_0\sin(\omega_y t)$ respectively, where ω_x, ω_y, x_0, y_0 are the designated value in the test (shown in Table 1). The velocities in the two translational directions can then be expressed as $\dot{x}(t) = \omega_x x_0\cos(\omega_x t)$, $\dot{y}(t) = \omega_y y_0\cos(\omega_y t)$ respectively. The aero-elastic coefficients of each layer caused by motion are calculated using the following formulae [10]:

$$K_{Lx}(z) = \frac{2}{Tq_zBH}\int_0^T F_{\mathrm{L}}(z,t)\frac{x(t)}{x_0}\mathrm{d}t \tag{3}$$

$$C_{Lx}(z) = \frac{2}{Tq_zBH}\int_0^T F_{\mathrm{L}}(z,t)\frac{\dot{x}(t)}{\omega_x x_0}\mathrm{d}t \tag{4}$$

$$K_{Dy}(z) = \frac{2}{Tq_zBH}\int_0^T F_{\mathrm{D}}(z,t)\frac{y(t)}{y_0}\mathrm{d}t \tag{5}$$

$$C_{Dy}(z) = \frac{2}{Tq_zBH}\int_0^T F_{\mathrm{D}}(z,t)\frac{\dot{y}(t)}{\omega_y y_0}\mathrm{d}t \tag{6}$$

where $F_{\mathrm{L}}(z,t)$ is the total wind force in the across-wind direction which contains the external load and the aero-elastic force; and $F_{\mathrm{D}}(z,t)$ is the total wind force in the along-wind direction. q_z is the reference pressure at height z, T is the sampling duration, and B is the windward width. The coefficients $K_{Lx}(z)$ and $C_{Lx}(z)$ represent the aerodynamic stiffness coefficient and the aerodynamic damping coefficient induced by the x axial motion respectively. $K_{Dy}(z)$ and $C_{Dy}(z)$ represent the aerodynamic stiffness coefficient and the aerodynamic damping coefficient induced by the y axial motion respectively.

The generalized aerodynamic damping (stiffness) force coefficients are computed by summing the aerodynamic elasticity coefficient of each layer of the structure, as follows:

$$K_{Lx} = \sum_{j=1}^{r} K_{Lx}(z_j)\varphi(z_j)\frac{\Delta_j}{H}\frac{q_j}{q_H} \tag{7}$$

$$C_{Lx} = \sum_{j=1}^{r} C_{Lx}(z_j)\varphi(z_j)\frac{\Delta_j}{H}\frac{q_j}{q_H} \tag{8}$$

$$K_{Dy} = \sum_{j=1}^{r} K_{Dy}(z_j)\varphi(z_j)\frac{\Delta_j}{H}\frac{q_j}{q_H} \tag{9}$$

$$C_{Dy} = \sum_{j=1}^{r} C_{Dy}(z_j)\varphi(z_j)\frac{\Delta_j}{H}\frac{q_j}{q_H} \tag{10}$$

where H is the height of the structure; r is number of total floors; $\varphi(z_j)$ is the mode shape at z_j, Δ_j is the layer height of the jth layer, q_j is the reference wind pressure at the jth layer, q_H is the reference wind pressure at the top of the model.

The aerodynamic damping ratios of the first two modes are calculated by:

$$\xi_{ax} = -\frac{1}{4}\frac{1}{x_0/H}\frac{\rho_a B^3}{M_n}\left(\frac{V_H}{2\pi f_x B}\right)^2 C_{Lx} \tag{11}$$

$$\xi_{ay} = -\frac{1}{4}\frac{1}{y_0/H}\frac{\rho_a B^3}{M_n}\left(\frac{V_H}{2\pi f_y B}\right)^2 C_{Dy} \tag{12}$$

where V_H is the wind speed at top of the model; M_n is the modal mass; for high rise buildings with uniform mass distribution along height and linear mode shape, the modal mass $M_n = \frac{1}{3}\rho_s BlH$; l is the downwind dimension, ρ_a and ρ_s are the densities of air and structure, respectively.

Let $\theta_{Hx} = x_0/H$ and $\theta_{Hy} = y_0/H$ as the x and y axial dimensionless

amplitude respectively, we have

$$\xi_{ax} = -\frac{3}{16\pi^2}\frac{\rho_a}{\rho_s}\left(\frac{V_H}{f_x B}\right)^2 \frac{C_{Lx}}{\theta_{Hx}} \tag{13}$$

$$\xi_{ay} = -\frac{3}{16\pi^2}\frac{\rho_a}{\rho_s}\left(\frac{V_H}{f_y B}\right)^2 \frac{C_{Dy}}{\theta_{Hy}} \tag{14}$$

The ratio of aero-elastic stiffness to structural stiffness defined as aerodynamic stiffness ratio can be calculated by

$$\frac{K_{ax}}{K_{sx}} = -\frac{3}{8\pi^2}\frac{\rho_a}{\rho_s}\left(\frac{V_H}{f_x B}\right)^2 \frac{K_{Lx}}{\theta_{Hx}} \tag{15}$$

$$\frac{K_{ay}}{K_{sy}} = -\frac{3}{8\pi^2}\frac{\rho_a}{\rho_s}\left(\frac{V_H}{f_y B}\right)^2 \frac{K_{Dy}}{\theta_{Hy}} \tag{16}$$

where K_{ax} and K_{ay} are x and y axial aerodynamic stiffness respectively; K_{sx} and K_{sy} are x and y axial structural stiffness respectively.

4.3. Complex aerodynamic impedance method (CAIM) for identification of aero elastic parameters

The aerodynamic impedance is defined as [12]:

$$K_A = -S_{yF}(f_y)/S_{yy}(f_y) \tag{17}$$

in which, $S_{yF}(f_y)$ is the value of cross spectrum of displacement and external force at the vibration frequency; $S_{yy}(f_y)$ is the value of displacement power spectrum at the vibration frequency, which is calculated by using the time histories of the displacement at the top of the model and the first order generalized force.

Aerodynamic impedance coefficient is obtained by non-dimensionalizing the aerodynamic impedance [12]

$$G_A = K_{A0}/(2\omega^2 M_n \eta) = \alpha + i\beta \tag{18}$$

where α and β are the real and imaginary parts of the aerodynamic impedance coefficient.

The formula for calculating the aerodynamic damping ratio is as follows:

$$\xi_a = \eta\beta \tag{19}$$

The formula for aerodynamic stiffness ratio (as defined before) is:

$$K_a/K_s = 2\eta\alpha \tag{20}$$

In the above formulas, $\eta = \rho_a/\rho_s$ is the ratio of the air density to the structural density.

5. Test results and analysis

5.1. Effect of vibration form on aerodynamic damping ratio

Fig. 8 compares the across-wind aerodynamic damping ratios of the square building identified by the bi-axial forced vibration test with those by the across-wind forced vibration test. It can be seen from Fig. 8 that there is a rather large difference between the identified across-wind aerodynamic damping ratios obtained by the bi-axial forced vibration and those by the forced vibration only in across-wind direction, especially when the reduced wind speed ranges from 11 to 14. That is to say, the across wind aerodynamic damping ratios of the structure are affected by along-wind structural vibrations. It can be concluded that the across-wind aerodynamic damping ratios identified by the bi-axial forced vibration are more accurate than those by the forced vibration only in across-wind direction.

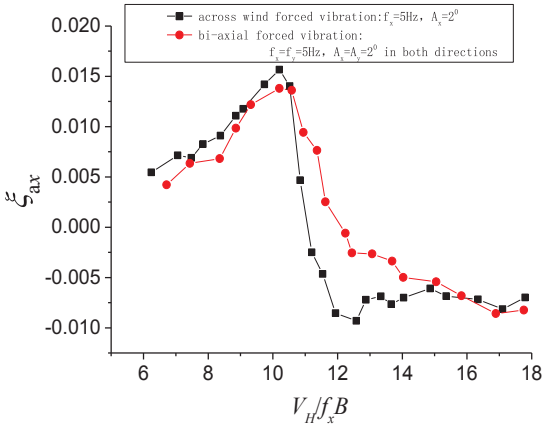

Fig. 8. Comparison of across-wind aerodynamic damping ratios identified by bi-axial and uniaxial forced vibration.

5.2. Effect of vibration amplitude on aerodynamic damping ratio

Table 1 in Section 3 sets 1.51 cm and 0.76 cm as the amplitudes at the top of the forced vibration model in across-wind and along-wind directions respectively. Actually, the wind-induced vibration amplitude of the high-rise building will not reach as large as that according to the geometry scale. Therefore, the influence of vibration amplitudes on aerodynamic damping ratio in across-wind direction was investigated in Figs. 9 and 10.

In Figs. 9 and 10, amplitude is quantified by the sway angle of the forced vibration device. For instance, A = 1.0° means that the amplitude at top of the building model equals 1.51 cm. Figs. 9 and 10 show that when along-wind or across-wind amplitude is fixed, the changes of across-wind or along-wind amplitude have little effect on across-wind aerodynamic damping ratio under various reduced wind speeds. In general, across-wind vibrations of high-rise buildings are much stronger than along-wind vibrations under strong wind. For this case, dynamic displacements in the across-wind direction are almost twice as much as those in along-wind direction under strong wind according to calculations based on wind pressure data measured on a rigid model in the wind tunnel. Therefore, considering the control precision of the forced vibration device, building top displacements of 1.51 cm and 0.76 cm were chosen as the vibration amplitudes of the forced vibration device in across-wind and along-wind directions respectively.

5.3. Analysis of wind force

The drag and lift force time histories of each layer were obtained by integrating the wind pressure of each pressure tap weighted by its attributed area in the same layer. Fig. 11 shows vibration displacement

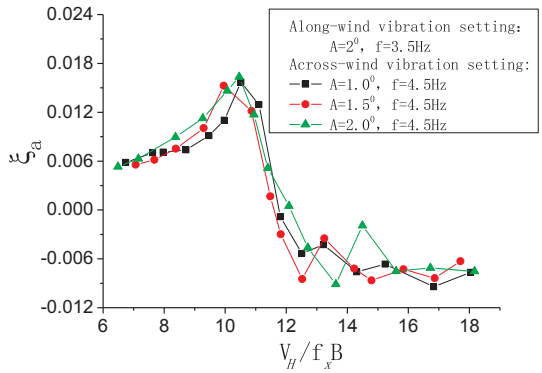

Fig. 9. The effect of across-wind amplitude on across-wind aerodynamic damping ratio.

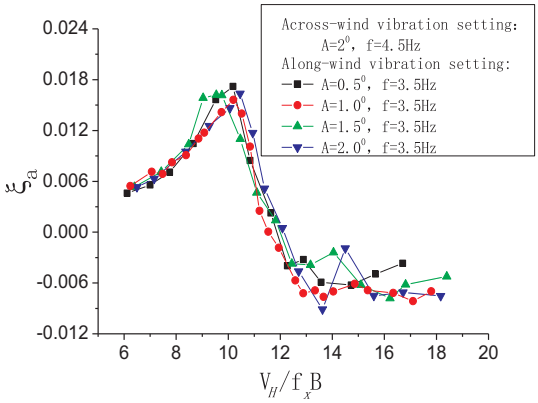

Fig. 10. The effect of along-wind amplitude on across-wind aerodynamic damping ratio.

time histories at the top of the model and wind force time histories. Fig. 11(a) shows varied phase difference between along-wind and across-wind displacement time histories. The initial phase difference between along-wind and across-wind displacements is determined by the initial position of the pole in the two directions as mentioned above. Because the vibration frequencies in along-wind and across-wind directions are different, the phase difference between along-wind and across-wind displacements changes with time. Therefore, the initial phase difference between along-wind and across-wind displacements has insignificant effects on the identification results of aerodynamic damping and aerodynamic stiffness ratios in the two directions. The time histories of drag and lift forces appear obviously periodic characteristics.

Fig. 12 shows the normalized lift force spectra of the typical layer (z = 69.5 cm), where each line represents the spectrum of a different reduced wind speed. In Fig. 12, the sharp vibration force peaks appear at the across-wind vibration frequencies for both case 1 and case 2. As is known to all, the Strouhal number for a square model is within 0.1–0.127 [19–21], whose reciprocal is in the range of 7.8–10. When reduced wind speed V_r is in the range of 7–10, which may be the reciprocal of Strouhal number of the building model as mentioned above, the vibration force peak is much higher for the vibration force has been associated with vortex shedding force. Fig. 13 shows the normalized drag spectra of the typical layer, in which there are dense turbulence wind force peaks at low frequency domain and sharp vibration force peaks at the along-wind vibration frequencies.

5.4. Identification of aerodynamic damping ratio and aerodynamic stiffness ratio

The curves of identified aerodynamic damping ratio and aerodynamic stiffness ratio in across-wind direction versus reduced wind speed are shown in Figs. 14 and 15. In these two figures, f_{1x} and f_{1y} represent the x axial vibration frequency and y axial vibration frequency of case one respectively; f_{2x} and f_{2y} represent x axial vibration frequency and y axial vibration frequency of case two respectively. The tendency of aerodynamic elastic parameters identified by the time domain integral method (TDIM) and the complex aerodynamic impedance method (CAIM) are consistent, which indicates that the identification methods of aero-elastic parameters by the forced vibration test are stable and effective. Fig. 16 shows the variation curve of the aerodynamic damping ratio versus the reduced wind speed in along wind direction, and according to calculation, the aerodynamic stiffness of the along-wind direction is minimal and can be ignored.

In Fig. 14, the curves of across-wind aerodynamic damping ratios for both case one and case two have sharp peaks when reduced wind speed is approaching to 10, and then dramatically drop to negative values when reduced wind speed is larger than 10. And in Fig. 15, the curves of across-wind aerodynamic stiffness ratios for both case one and case two dramatically decrease when reduced wind speed is larger than 6, then reach minimum negative values near 10. As reduced wind speed gradually increases, the curves of across-wind aerodynamic stiffness ratios steeply rise, forming sharp valleys. Apparently, the shapes of the curves of across-wind aerodynamic damping and aerodynamic stiffness ratios based on wind tunnel data of the bi-axial forced vibration device are consistent with those results based on wind tunnel data of the unidirectional forced vibration device [12] and the multi-degree-of-freedom aerodynamic model [22–24]. It is not hard to find that the significant changes of the curves of across-wind aerodynamic damping ratios and aerodynamic stiffness ratios occur when reduced wind speeds are close to even equal to critical wind speed of vortex induced resonance, which is the reciprocal of Strouhal number. As mentioned above, the reciprocal of the Strouhal number for a square building is in the range of 7.8–10. The building model in this experiment is a quasi square model, thus it is reasonable that the undulating domains of the curves of across-wind aerodynamic damping and aerodynamic stiffness ratios are within reduced wind speed 6–14. Vortex shedding as well as vortex-induced vibration are unsteady phenomena in flow dynamics and structural dynamics [22,25]. Actually, vortex shedding coupled with structural vibration frequency is the main reason to make the curves of across-wind aerodynamic damping and aerodynamic stiffness ratios undulate. Nevertheless, the variation mechanism of the curves of

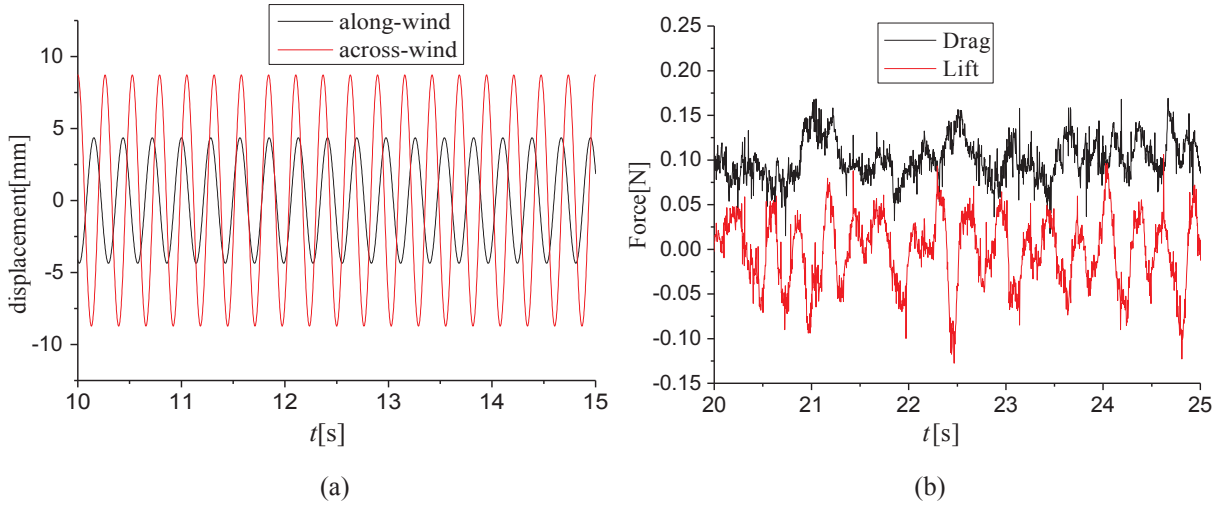

Fig. 11. Time history curve: (a) displacement at top of the model; (b) force on the model.

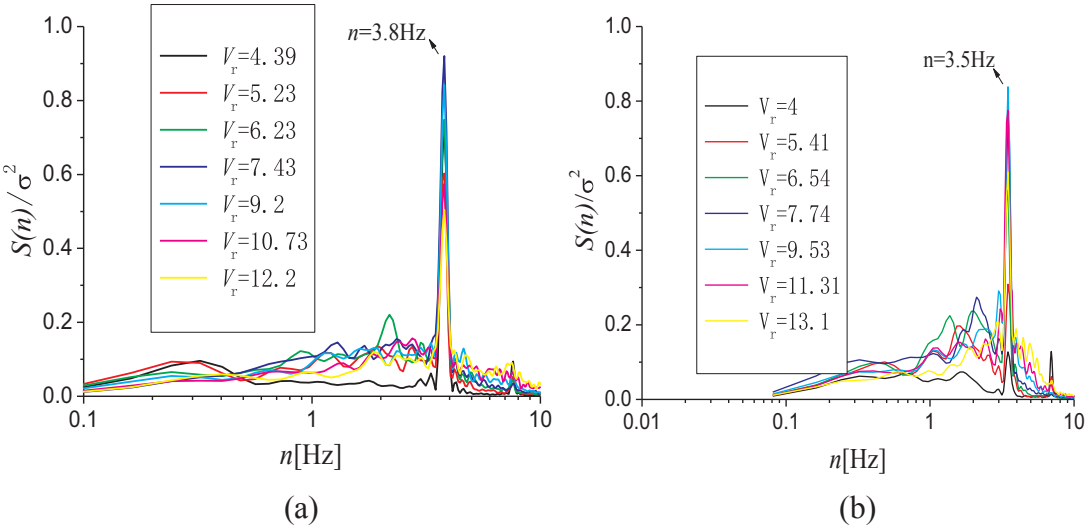

Fig. 12. Normalized lift spectra of typical layer (z = 69.5 cm): (a) case one; (b) case two.

across-wind aerodynamic damping and aerodynamic stiffness ratios in the reduced wind speed domain of vortex induced vibration are still not clear, and need further exploration [22].

According to Figs. 14–16, the aerodynamic damping ratio and aerodynamic stiffness ratio of the structure can be estimated and therefore the frequency response function can be improved.

5.5. Structural dynamic characteristic correction

Based on the identified aerodynamic damping ratio and aerodynamic stiffness ratio, the structural frequency and structural damping ratio are corrected as

$$f_s' = \frac{1}{2\pi}\sqrt{\frac{K}{M}} = \frac{1}{2\pi}\sqrt{\frac{K_S + K_a}{M}} = f_S\sqrt{1 + \frac{K_a}{K_S}} \tag{21}$$

$$\xi_s' = \xi_s + \xi_a \tag{22}$$

where f_s is the structural natural frequency, $f_s^{'}$ is the modified structural frequency. ξ_s is structural damping ratio, ξ_s' is modified structural damping ratio, K_a is the aerodynamic stiffness, K_s is the structural stiffness.

Table 2 lists the results of the modified dynamic characteristics of the structure for different return periods. f_{s1}' and f_{s2}' are the modified 1st and 2nd order frequencies of the structure respectively. ξ_{ax} and ξ_{ay} are the 1st and 2nd order aerodynamic damping ratios respectively. The modified frequencies and aerodynamic damping ratios in Table 2 are acquired in accordance with Figs. 14 and 15 and Eqs. (21) and (22), where the wind speeds V_H for different return periods are determined by local design wind pressure in Chinese code [16]. It can be seen from Table 2 that the variation of across wind frequency is very small, and the aerodynamic damping ratios in across-wind direction are greater than those in along-wind direction.

5.6. Calculation results of dynamic response

Table 3 shows the maximum displacement and acceleration responses at the top of the high-rise building. According to China's code [16], as mentioned above, in Table 3 and Figs. 17 and 18, the structural damping ratio for displacement and equivalent static wind load calculation is 0.02. For acceleration calculation, the structural damping ratio is 0.015 to guaranty that discomfort of building occupants will not be underestimated. The X-axis and Y-axis are defined the same as those in Fig. 2.

As can be seen from Table 3, considering the aerodynamic damping ratio, the maximum displacement responses at the top of the building and the maximum acceleration responses at the highest residential layer are reduced. The displacement reduction coefficient of aeroelastic effect μ_d is defined by the ratio of the displacement regard for

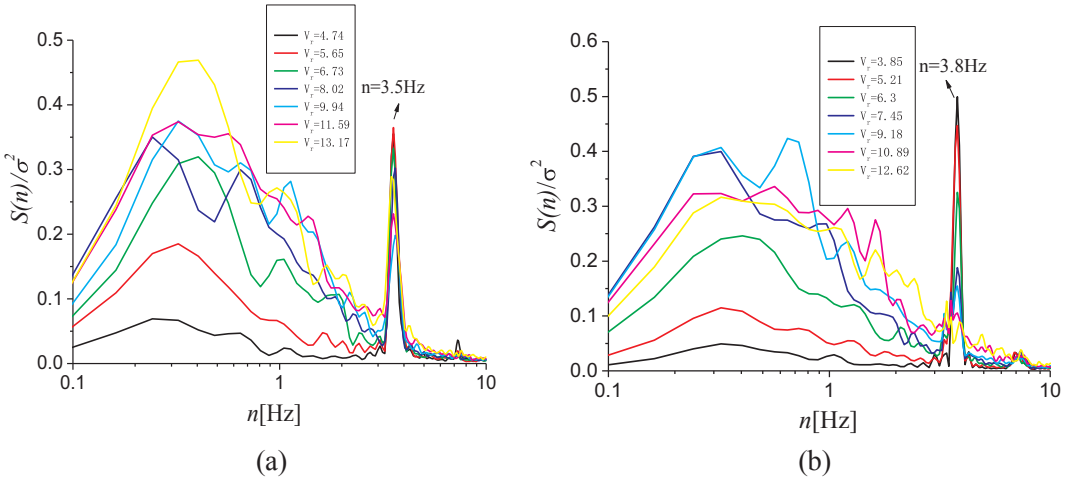

Fig. 13. Normalized drag spectra of typical layer (z = 69.5 cm) : (a) case one; (b) case two.

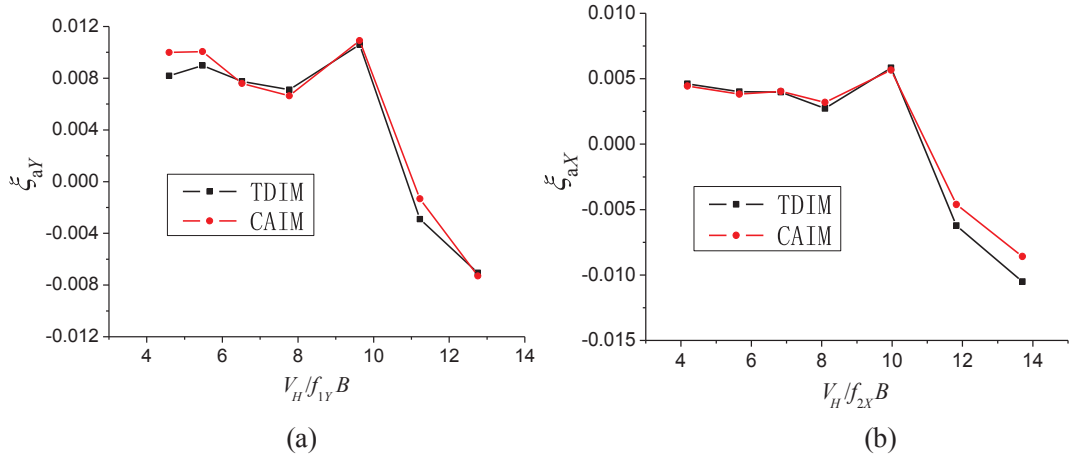

Fig. 14. Across-wind aerodynamic damping ratios: (a) case one; (b) case two.

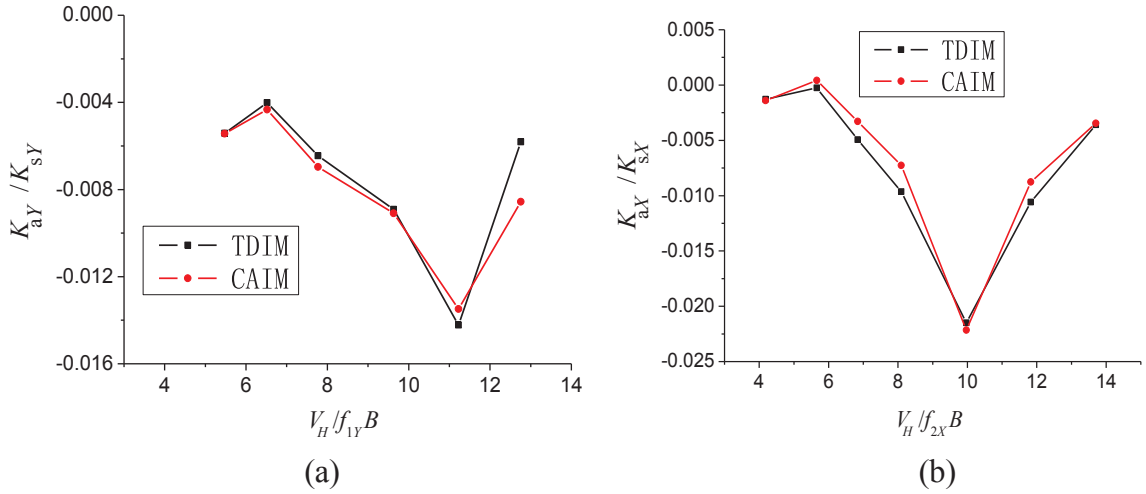

Fig. 15. Across-wind aerodynamic stiffness ratios: (a) case one; (b) case two.

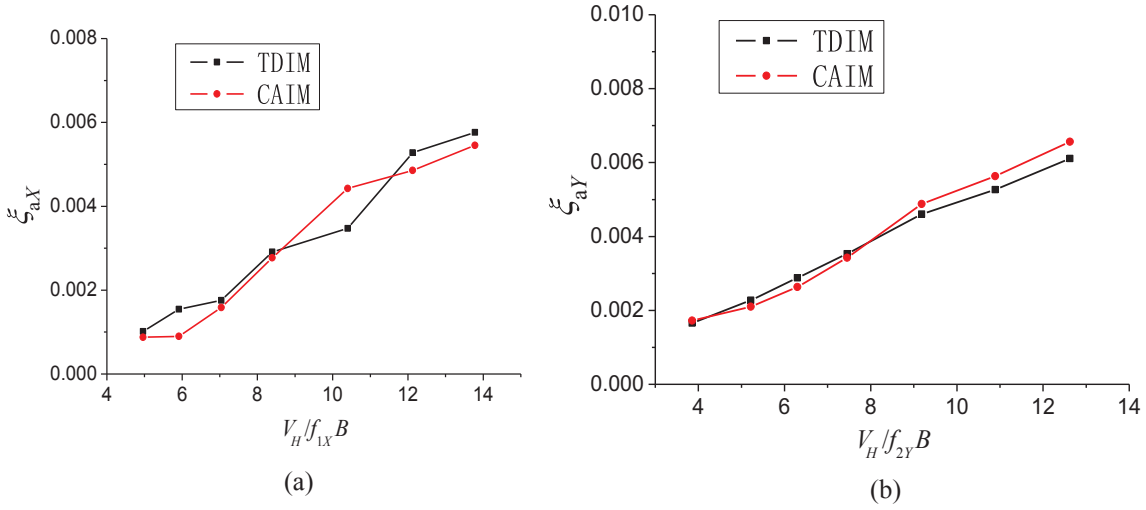

Fig. 16. Along-wind aerodynamic damping ratios: (a) case one; (b) case two.

aero-elastic effect to the displacement without regard for aero-elastic effect. In addition, the acceleration reduction coefficient of aero-elastic effect μ_a is defined by the ratio of the acceleration regard for aero-elastic effect to the acceleration without regard for aero-elastic effect. As shown in Table 4, the maximum displacement response has been reduced by 4% and the maximum acceleration response by 10% after consideration of the aero-elasticity effect.

The equivalent static wind load was calculated by using the mode acceleration method based on the internal force equivalence proposed in Ref. [26]. Figs. 17 and 18 show the equivalent static wind loads at

Table 2
Correction of structural dynamic characteristics.

Return period	n = 10 years (V_H = 32.25)				n = 50 years (V_H = 38.12)				n = 100 years (V_H = 40.79)			
	f'_{s1} [Hz]	ξ_{ax}	f'_{s2} [Hz]	ξ_{ay}	f'_{s1} [Hz]	ξ_{ax}	f'_{s2} [Hz]	ξ_{ay}	f'_{s1} [Hz]	ξ_{ax}	f'_{s2} [Hz]	ξ_{ay}
Case one	0.175	0.001	0.1894	0.009	0.175	0.0013	0.1895	0.009	0.175	0.0015	0.1895	0.0085
Case two	0.1749	0.00425	0.19	0.0018	0.1749	0.004	0.19	0.0023	0.1748	0.004	0.19	0.0025

wind directions of 90°and 180° respectively for 50 year recurrence period. The red and black lines indicate the equivalent static wind load with and without aero-elasticity effect modification (AEEM), respectively. It can be seen that for both wind directions of 90° and 180°, the along-wind equivalent static wind loads with or without the aero-elasticity effect are almost the same. However, for the across-wind equivalent static wind load, especially at the middle and upper parts of the building, the equivalent static wind loads considering aero-elastic effects decrease slightly.

Based on the equivalent static wind loads on each layer for the 50-year recurrence period, the shear force and bending moment of the structure are calculated, and the reduction coefficients of the aero-elastic effect of the shear force and bending moment of the structure are also calculated, as shown in Table 5. As can be seen, for both wind directions of 90° and 180°, the reduction coefficients of the aero-elastic effect of the base shear forces and bending moments in across-wind direction are about 0.97, while the reduction coefficients of the aero-elastic effect of the base shear forces and bending moments in along-wind direction are about 0.997. Therefore, the aero-elastic effect reduction coefficients of the total base shear force and the total base bending moment are about 0.988. The aero-elastic effect reduction coefficients of the total base bending moment are slightly less than those of the total base shear force, because the reduction of the equivalent static wind loads at the middle and upper parts of the building is more significant than that at the lower parts after consideration of the aero-elasticity effect.

This investigation shows that for high-rise buildings with a height more than 300 m, the influence of aero-elastic effect on their wind vibration responses should be considered. The bi-axial forced vibration wind tunnel test is a stable, reliable and practical method to identify the aero-elastic parameters of high-rise flexible structures. The identified parameters can be used to improve the accuracy of predicted wind vibration responses based on the surface wind pressure data of a rigid model test. Furthermore, the wind tunnel tests using this device are less complicated and more efficient than multi-degree-of freedom (MDOF) aero-elastic model tests.

When the height of a tall building is more than 600 m, the fundamental frequency of the building is less than 0.1, and the aspect ratio of the building is more than 10, its aero-elastic effects may increase significantly. For those super slenderer, more flexible tall buildings, motion-induced variation of vibration characteristics, responses as well as wind field of the buildings probably could not be evaluated accurately by using the bi-axial forced vibration device because of the error induced by linear vibration mode shapes and neglecting torsional movement of the device. It is anticipated that a 3D forced vibration wind tunnel test which considers the torsional vibration and linear mode shape correction could be a powerful means to indentify aero-elastic parameters and effects for those super slenderer, more flexible tall buildings accurately.

6. Conclusions

Based on the bi-axial forced vibration test of Changsha Shimao Plaza model, the aerodynamic elastic parameters of the building were identified. Furthermore, the effects of aerodynamic damping ratio and aerodynamic stiffness on the wind-induced displacements, accelerations as well as equivalent static wind loads of the structure were examined. The following conclusions have been drawn:

1. The bi-axial forced vibration wind tunnel test is an effective approach to identify aero-elastic effects of wind-induced vibrations of high-rise buildings, which can take the correlation between the vibrations in two horizontal orthogonal directions into consideration. In addition, the bi-axial forced vibration wind tunnel test is a more

Table 3
Maximum displacement and acceleration of the structure.

Case No.	Direction and position	Top			Highest residential layer		
		d_{10} [m]	d_{50} [m]	d_{100} [m]	a_{10} [m·s^{-2}]	a_{50} [m·s^{-2}]	a_{100} [m·s^{-2}]
1_a	X axis	0.13147	0.18560	0.21553	0.04415	0.06354	0.0778
	Y axis	0.08931	0.13975	0.17303	0.07326	0.12604	0.16573
	center	0.17482	0.25712	0.30736	0.08554	0.14116	0.18308
	corner	0.17597	0.25870	0.30925	0.09189	0.14801	0.19220
1_b	X axis	0.13078	0.18473	0.21437	0.04288	0.06203	0.07577
	Y axis	0.08527	0.13157	0.16109	0.06223	0.10560	0.13793
	center	0.17129	0.25015	0.29699	0.07557	0.12247	0.15737
	corner	0.17245	0.25174	0.29891	0.08270	0.13031	0.16789
2_a	X axis	0.09005	0.15180	0.17834	0.07239	0.13831	0.16086
	Y axis	0.10898	0.15123	0.17639	0.04281	0.05699	0.07062
	center	0.15732	0.24104	0.28266	0.08410	0.14960	0.17568
	corner	0.15967	0.24432	0.28641	0.08774	0.15440	0.18149
2_b	X axis	0.08579	0.14191	0.16783	0.06327	0.11955	0.14128
	Y axis	0.10815	0.15030	0.17512	0.04096	0.05500	0.06808
	center	0.15317	0.23158	0.27234	0.07537	0.13159	0.15683
	corner	0.15552	0.23489	0.27612	0.07941	0.13703	0.16331

Note: the subscripts a and b of Case No. mean without considering and considering aero-elastic effect respectively, and the subscripts 10, 50 and 100 of displacement d and acceleration a mean return period.

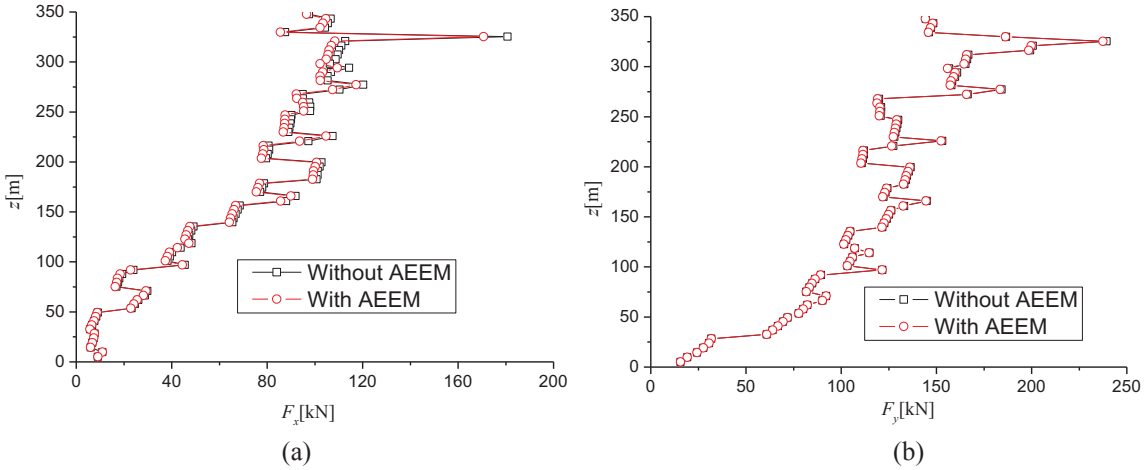

Fig. 17. Equivalent static wind load at wind direction of 90°: (a) X axial (across-wind direction) equivalent wind load; (b) Y axial (along-wind direction) equivalent wind load.

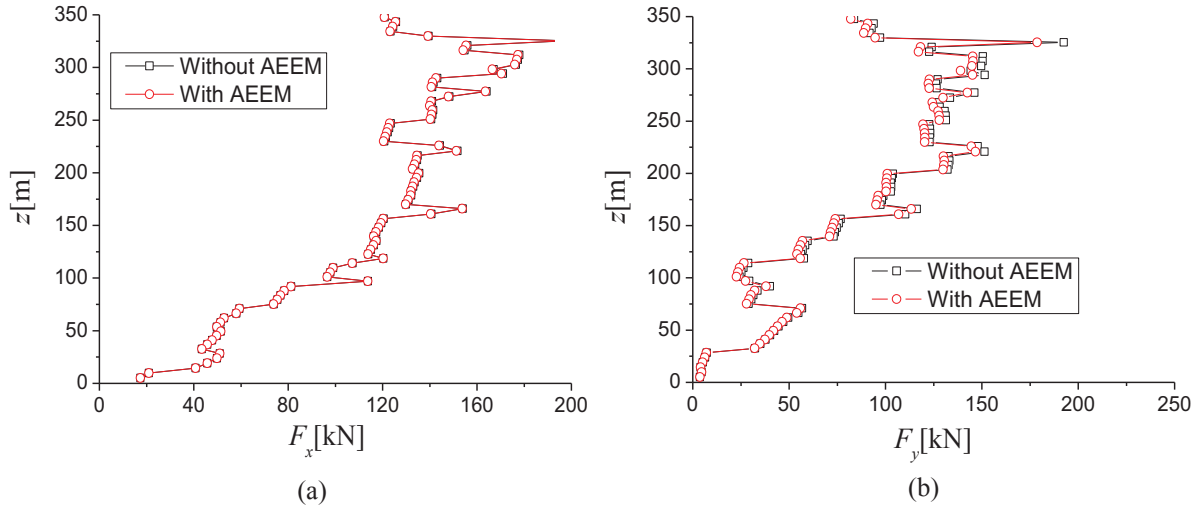

Fig. 18. Equivalent static wind load at wind direction of 180°: (a) X axial (along-wind direction) equivalent wind load; (b) Y axial (across-wind direction) equivalent wind load.

Table 4
Aero-elastic effects reduction factors of wind-induced responses.

Case	Reduction factors	Direction and position	Recurrence period		
			10-year	50-year	100-year
1	μ_d	X axis	0.99475	0.99531	0.99462
		Y axis	0.95476	0.94147	0.93099
		center	0.97981	0.97289	0.96626
		corner	0.98000	0.97310	0.96656
1	μ_a	X axis	0.97123	0.97624	0.97391
		Y axis	0.84944	0.83783	0.83226
		center	0.88345	0.86760	0.85957
		corner	0.89999	0.88041	0.87352
2	μ_d	X axis	0.95269	0.93485	0.94107
		Y axis	0.99238	0.99385	0.99280
		Center	0.97362	0.96075	0.96349
		corner	0.97401	0.96140	0.96407
2	μ_a	X axis	0.87402	0.86436	0.87828
		Y axis	0.95679	0.96508	0.96403
		center	0.89620	0.87961	0.89270
		corner	0.90506	0.88750	0.89983

rational approach to identify aero-elastic effects than the unidirectional forced vibration wind tunnel test.

2. Based on the linear assumption of aerodynamic elastic force, the along-wind and across-wind aerodynamic damping ratios, and across-wind aerodynamic stiffness ratio of Changsha Shimao Plaza wind tunnel model were identified by time domain integral method and complex aerodynamic impedance method, respectively. The results obtained by these two methods agree well with each other, which proves that the aero-elastic parameter identification methods are reliable and effective.
3. Under the extreme wind speed of 100-year recurrence period, the along-wind and across-wind aerodynamic damping ratios of the high-rise building in the two typical wind directions are positive. After considering the aerodynamic damping, the wind-induced dynamic responses of the structure will be reduced slightly. Aerodynamic stiffness has little effect on the natural frequency of the structure. Considering the aerodynamic stiffness, the self-vibration frequency of the across-wind direction of the structure slightly decreases.
4. The aerodynamic elastic effect cannot be ignored for wind-induced responses of Changsha Shimao Plaza under strong wind, especially for the acceleration responses. The aerodynamic elastic effect reduction coefficient of the maximum displacement response at the

Table 5
Aero-elastic effects reduction coefficients of equivalent static wind loads.

	Basal internal force	Whether to consider the aerodynamic elastic effect		Reduction coefficient
		not considering	considering	
Case one	X-axis shear Q_x [kN]	9.370×10^3	9.340×10^3	0.9967
	Y-axis shear Q_y [kN]	5.480×10^3	5.330×10^3	0.9725
	Total shear Q_t [kN]	1.138×10^4	1.124×10^4	0.9876
	X axis bending moment M_x [kN m]	1.946×10^6	1.939×10^6	0.9961
	Y axis bending moment M_y [kN m]	1.254×10^6	1.218×10^6	0.9713
	Total bending moment M_t [kN m]	2.426×10^6	2.392×10^6	0.9860
Case two	X-axis shear Q_x [kN]	6.870×10^3	6.660×10^3	0.9698
	Y-axis shear Q_y [kN]	9.070×10^3	9.050×10^3	0.9977
	Total shear Q_t [kN]	1.085×10^4	1.075×10^4	0.9906
	X axis bending moment M_x [kN m]	1.533×10^6	1.485×10^6	0.9687
	Y axis bending moment M_y [kN m]	1.881×10^6	1.876×10^6	0.9973
	Total bending moment M_t [kN m]	2.315×10^6	2.289×10^6	0.9889

top of the building under the extreme wind speed of 100-year recurrence period is about 0.96, and the aerodynamic elastic effect reduction coefficient of the maximum acceleration response at the highest residential layer of the building under the extreme wind speed of 100-year recurrence period is about 0.90. While the aerodynamic elasticity effect reduction coefficients of the total base shear and the total base bending moment under the extreme wind speed of 100-year recurrence period calculated by the equivalent static wind loads are about 0.99.

This investigation shows that for high-rise buildings with a height more than 300 m, the influence of aero-elastic effect on their wind vibration responses should be considered. The bi-axial forced vibration wind tunnel test is a stable, efficient, convenient and practical method to identify the aero-elastic parameters of high-rise flexible structures. The identified parameters can be used to improve the accuracy of predicted wind vibration responses based on the surface wind pressure data of a rigid model test.

Acknowledgments

The investigation presented in this paper was supported by the China National Natural Science Foundation under project No. 50678137, which is gratefully acknowledged.

References

[1] Kareem A, Gurley K. Damping in structures: its evaluation and treatment of uncertainty. J Wind Eng Ind Aerodyn 1996;59:131–57.
[2] Huang Peng, Quan Yong, Gu Ming. Experimental study of aerodynamic damping of typicaltall buildings. Math Problems Eng 2013;2013:1–9.
[3] Hu G, Hassanli S, Kwok KCS, Tse KT. Wind-induced responses of a tall building with a double-skin façade system. J Wind Eng Ind Aerodyn 2017;168:91–100.
[4] Gu M, Cao HL, Quan Y. Experimental study of across-wind aerodynamic damping of super high-rise buildings with aerodynamically modified square cross-sections. Struct Des Tall Special Build 2014;23:1225–45.
[5] Cheng CM, Lu PC, Tsai MS. Across-wind aerodynamic damping of isolated square-shaped buildings. J Wind Eng Ind Aerodyn 2002;90(12–15):1743–56.
[6] Tamura Y, Suganuma SY. Evaluation of amplitude-dependent damping and natural frequency of buildings during strong winds. J Wind Eng Ind Aerodyn 1996;59(2–3):115–30.
[7] Kato N, Marukawa H, Fujii K, et al. Experimental evaluation of aerodynamic damping of tall buildings. J Wind Eng Ind Aerodyn 1996;59(2–3):177–90.
[8] Vickery BJ, Steckley A. Aerodynamic damping and vortex excitation on an oscillating prism in turbulent shear flow. J Wind Eng Ind Aerodyn 1993;49(1–3):121–40.
[9] Fediw AA, Nakayama M, Cooper KR, et al. Wind tunnel study of an oscillating tall building. J Wind Eng Ind Aerodyn 1995;57(2–3):249–60.
[10] Chen Ruohua, Zheng Qiming, Bojian LU. Wind-structure interaction of a high-rise building in boundary layer flows. J Chinese Inst Civil Hydraulic Eng 1997;9(2):271–9.
[11] Cooper KR, Nakayama M, Sasaki Y, et al. Unsteady aerodynamic force measurements on a super-tall building with a tapered cross section. J Wind Eng Ind Aerodyn 1997;72(1–3):199–212.
[12] Steckley S. Motion induced wind forces on chimneys and tall buildings. London: The University of Western Ontario; 1989. p. 67–137.
[13] Katagiri J, Ohkuma T, Marikawa H. Motion-induced wind forces acting on rectangular high-rise buildings with side ratio of 2. J Wind Eng Ind Aerodyn 2001;89:1421–32.
[14] Katagiri J, Ohkuma T, Marukawa H. Analytical method for coupled across-wind and torsional wind responses with motion-induced wind forces. J Wind Eng Ind Aerodyn 2002;90:1795–805.
[15] Liang Shuguo, Li QS, Li Guiqing, et al. An evaluation of onset wind velocity for 2-D coupled galloping oscillations of tower buildings. J Wind Eng Ind Aerodyn 1993;50:329–39.
[16] Chinese Code. Lode code for the design of building structures 2012; GB50009-2012.
[17] Liang Shuguo, Zou Lianghao, Peng Xiaohui, et al. Dynamic wind loads on tall building models undergoing bi-axial forced vibration in wind tunnel test. In: The 13th international conference on wind engineering, Amsterdam, Netherlands. Multi-Science Publishing Co Ltd; 2011. p. 1055–62.
[18] Simiu E, Scanlan RH. Wind effects on structures. John Wiley and Sons Ltd; 1986.
[19] Amandolèse X, Hémon P. Vortex-induced vibration of a square cylinder in wind tunnel. C R Mec 2010;338:12–7.
[20] Hayashida H, Iwasa Y. Aerodynamic shape effects of tall building for vortex induced vibration. J Wind Eng Ind Aerodyn 1990;33:237–42.
[21] Eurocode: Basis of design and actions on structures 1991; Part 2-4: wind action, Page 133.
[22] Wang L, Liang S, Huang G, Song J, Zou L. Investigation on the unstability of vortex induced resonance of high-rise buildings. J Wind Eng Ind Aerodyn 2018;175:17–31.
[23] Wang L, Fan XY, Liang Shuguo, Wang J, Song ZK. Improved expression for across-wind aerodynamic damping ratios of super high-rise buildings. J Wind Eng Ind Aerodyn 2018;176:263–72.
[24] Wang L, Liang Shuguo, Song J, Wang S. Analysis of vortex induced vibration frequency of super tall building based on wind tunnel tests of MDOF aero-elastic model. Wind Struct 2015;21(5):523–36.
[25] Blevins RD. Flow induced vibration. 2nd ed. Krieger Publishing Company; 2006.
[26] Liang Shuguo, Zou Lianghao, Wang Dahai, et al. Analysis of three dimensional equivalent static wind loads of symmetrical high-rise buildings based on wind tunnel tests. Wind Struct 2014;19(5):565–83.